Title: Tgfbi/Bigh3 silencing activates ERK in mouse retina.
Authors: Allaman-Pillet N, Oberson A, Bustamante M, Tasinato A, Hummler E, Schorderet DF
Journal: Experimental eye research
Year: 2015 Nov
Volume: 140
Pages: 159-70
DOI: 10.1016/j.exer.2015.09.004

Tgfbi/Bigh3 silencing activates ERK in mouse retina

Nathalie Allaman-Pillet[1], Anne Oberson[1], Mauro Bustamante[1], Andrea Tasinato[1], Edith Hummler[2,3]Daniel F. Schorderet[1,4]

1. Institut de Recherche en Ophtalmologie, Sion, Switzerland
2. Centre Hospitalier Universitaire Vaudois, Lausanne, Switzerland
3. Université de Lausanne, Lausanne, Switzerland
4. Ecole polytechnique fédérale de Lausanne, Faculté des Sciences de la vie, Lausanne, Switzerland

Corresponding Author: Dr Nathalie Allaman-Pillet, PhD

IRO, Institute for Research in Ophthalmology,

1950 Sion,

Switzerland

Phone : +41 27 205 79 03

Fax : +41 27 205 79 01

nathalie.allaman-pillet@irovision.ch

Keywords: BIGH3/TGFBi, retina, cornea, ERK, apoptosis

Abstract

BIGH3 is a secreted protein, part of the extracellular matrix where it interacts with collagen and integrins on the cell surface. BIGH3 can play opposing roles in cancer, acting as either tumor suppressor or promoter, and its mutations lead to different forms of corneal dystrophy. Although many studies have been carried out, little is known about the physiological role of BIGH3. Using the cre-loxP system, we generated a mouse model with disruption of the *Bigh3* genomic locus. *Bigh3* silencing did not result in any apparent phenotype modifications, the mice remained viable and fertile.

We were able to determine the presence of BIGH3 in the retinal pigment epithelium (RPE). In the absence of BIGH3, a transient decrease in the apoptotic process involved in retina maturation was observed, leading to a transient increase in the INL thickness at P15. This phenomenon was accompanied by an increased activity of the pro-survival ERK pathway.

Introduction

BIGH3, also known as *TGFBI* (Transforming growth factor-ß-induced), encodes a 68-kDa protein expressed in most human tissues, but not in the brain (Skonier et al., 1992; LeBaron et al., 1995; Bae et al., 2002; Ferguson et al., 2003). BIGH3 is secreted and accumulates in the extracellular matrix (ECM). Through four fasciclin-1 (FAS1) domains and a carboxy-terminal Arg-Gly-Asp (RGD) motif, BIGH3 binds molecules of the ECM, including fibronectin, laminin and different collagens (Hashimoto et al., 1997; Hanssen et al., 2003) and serves as a ligand for several integrins, including aVβ3 and aVβ5 (Billings et al., 2002; Hanssen et al., 2003; Reinboth et al., 2006; Ferguson et al., 2003; Kim et al., 2002; Kim et al., 2000; Nam et al., 2006). It is therefore assumed that BIGH3 modulates cell-cell adhesion, as well as cell-ECM interaction. Studies in cell culture have also displayed the potential role of BIGH3 in apoptosis induction (Morand et al., 2000; Kim et al., 2003; Zamilpa et al., 2009). The C-terminal 69 amino acids of BIGH3 containing the RGD peptide motif seems essential for triggering apoptosis, which implicates an integrin-mediated process (Kim et al., 2003; Zamilpa et al., 2009).

BIGH3, when mutated or expressed at an abnormal level, is associated with various pathologies. Numerous studies have shown that BIGH3 plays a role in cancer progression, with a function of tumor promoter or suppressor depending on the tissue (Sasaki et al., 2002; Hourihan et al., 2003; Hu et al., 2001; Zajchowski et al., 2001; Notterman et al., 2001; Zhao et al., 2003). In the human cornea, where BIGH3 is abundantly expressed, its mutated forms are associated with corneal dystrophies, a group of inherited diseases characterized by amyloid or non-amyloid deposits in various layers of the cornea. (Munier et al., 1997; Korvatska et al., 2000). Although BIGH3 is ubiquitously expressed, BIGH3 deposits occur only in corneas, leaving the other tissues intact (Elkochairi et al.,2006).

In order to further clarify the role of BIGH3 in development and in the eye, we generated a *Bigh3* deficient mouse model using the Cre-loxP method, a site-specific recombinase technology widely used to carry out deletions, insertions, translocations and inversions at specific sites in the DNA (Sauer et al., 1998).

Material and Methods

Chemicals.

Primary antibodies used for western blotting and immunohistochemistry experiments were as followed : rabbit anti-BIGH3 (Proteintech Group, Chicago, IL, USA; #10188-1-AP) designed from the amino acids 199-406 encompassing exon 5 to 9, rabbit anti-KE2 (Korvatska et al., 2000) designed from the amino acids 426-682 encompassing exon 10 to 17, mouse anti-ERK (Cell Signaling Technology Inc., Danvers, MA, USA; #9101S), mouse anti-P-ERK (Cell Signaling; #4377S), mouse anti-AKT (Santa Cruz Biotechnologies Inc., Dallas, TE, USA; sc-5298), rabbit anti-P-AKT (Cell Signaling; #4060), rabbit anti-CCND1 (Santa Cruz; sc-718), rabbit anti-Ki67 (Abcam, Cambridge, UK; ab66155), rabbit anti-BCL-2 (Cell Signaling; #2876), rabbit anti-BCL-X_L (Cell Signaling; #2764), rabbit anti-BAX (Santa Cruz; sc-493), rabbit anti-BIM (Cell Signaling; #2819), rabbit anti-PUMA (Cell Signaling; #4976), mouse anti-EZR (Santa Cruz; sc-58758), mouse anti-RPE65 (Abcam; ab13826), rabbit anti-GAPDH (Santa Cruz; sc-25778), and mouse anti-ß-actin (Sigma, St. Louis, USA; A5441).

Anti-BIGH3 from Proteintech was used for both immunostaining and western blot, while anti-KE2 was used only for western blotting, as it does not function for immunostaining.

The secondary antibodies used for western blotting and immunohistochemistry experiments were as followed, goat anti-rabbit HRP or goat anti-mouse HRP (Amersham Biosciences,

Otelfingen, Switzerland) and Alexa Fluor 594 goat anti-rabbit or Alexa-Fluor 488 goat anti-mouse (Molecular Probes, Invitrogen Inc., Eugene, OR, USA).

Generation of Bigh3 knockout mouse.

The targeting vector was produced as shown in figure 1.A. A 6.2 kb mouse genomic DNA fragment containing the 5' regulatory region, exon 1 and part of intron 1 of the *Bigh3* gene was amplified from 129Sv/Ev genomic DNA by PCR and cloned. The fragments were then subcloned to introduce two loxP and two frt sites. A loxP sequence was inserted in the 5' regulatory region and a frt-PGKNeo-frt-loxP cassette was inserted in intron 1. Thus a fragment of 1640 bp genomic DNA encompassing exon 1 was floxed. An ATG depleted region resulted from the action of Cre recombinase (Fig 1.A).

The targeting vector was linearized and transfected into embryonic stem (ES) cells of the 129Sv/Ev background as described previously (Hummler et al., 1996). G418 and ganciclovir-resistant colonies were expanded and screened by PCR. The primer set Big1-F 5'-GGATCCAGCCCGCACTTGAC-3' and Neo-R 5'-AAGAACTCGTCAAGAAGGCGATAGAAGGCG-3' generated a PCR product of 5175 bp for the 5' region of the construct and the primer set Neo-F 5'-TTCTCCGGCCGCTTGGGT-3' and Big1-R 5'-CTCCAATAAGTCCGGAAAAGCA-3' generated a PCR product of 3200 bp for the 3' region of the construct (Fig 1.B-C). Three independent correctly targeted clones were obtained and injected into blastocysts of C57BL/6N mice. Chimeric mice were obtained that transmitted the floxed allele to their offspring (*Bigh3*$^{lox/+}$). To generate *Bigh3*$^{-/-}$ mice, *Bigh3*$^{lox/+}$ mice were crossed with Nestin-Cre transgenic mice, which express the Cre recombinase under the control of the nestin promoter active in the germ line (Buchholz et al., 1999). *Bigh3*$^{-/+}$ mice were obtained and backcrossed with C57BL/6N mice (>9 generations) to generate *Bigh3*$^{-/-}$ mice. Genotyping was carried out by PCR and confirmed by Southern blot analysis (Fig 1.D-F). *Bigh3* deficient

and wild type mice were tested for the Rd8 mutation, accordingly to previously described protocol (Chang et al., 2013) (Supplementary Fig S1).

Mice were maintained and euthanized in accordance with the ARVO Statement for the Use of Animals in Ophthalmic and Vision Research and were approved by the local Committee Office on Use and Care of Animals in Research of the State of Valais, Sion, Switzerland.

Genomic DNA extraction

Cut tail samples were incubated overnight in lysis buffer (100 mM TrisHCl, pH 8.5; 5 mM EDTA; 0.2 % SDS; 200 mM NaCl and 100 µg proteinase K per ml) at 56° C. After complete lysis, samples were centrifuged for 2 min and supernatant was transferred into isopropanol. After centrifugation, supernatant was removed and the pellet was resuspended in 150 µl 10 mM TrisHCl and 0.1 mM EDTA, pH 7.5, and incubated at 60° C for 10 min. The genomic DNA obtained was directly used to perform PCRs.

Genotyping by PCR

Genotyping through PCR was performed with obtained gDNA using the following primers: Big2-F 5'-GGATTCCTGAATGCCAAGGTG-3' and Big2-R 5'-CCCGGACCTTAGCTGAGCC-3'. Touchdown PCR was performed with LA Taq (Takara Bio Inc., Shiga, Japan) with the following amplification conditions: a first amplification step of 20 cycles consisting of 95° C 30 sec, 68° C 30 sec and 72° C 5min with diminishing annealing temperature of 0.5° C per cycle; then a second amplification step of 30 cycles as follows: 95° C 30 sec, 57° C 30 sec and 72° C 5 min; and a final elongation step of 10 min at 72° C. *Bigh3* WT and KO alleles were diagnosed on a 1 % agarose gel as 2290-bp and 690-bp amplified products, respectively.

Southern blot analysis

Genomic DNA obtained as described above was digested with BamHI overnight at 37° C. Southern blot (Sambrook et al., 1989) using a DIG-labelled probe was performed on digested

DNA following manufacturer's instructions (Roche Applied Science, Rotkreus, Switzerland). Briefly, digested DNA was separated on an agarose gel at 80 V for 4 h and then transferred into a positively charged nylon membrane (Roche) overnight. The membrane was then hybridized overnight with a specific DIG-labelled probe at 50° C. DIG was then detected with an anti-DIG antibody (1/10,000) and detected with the chemiluminescent substrate CSPD (Roche). Images were taken using LAS-4000mini Luminescent Image Analyzer (FujiFilm, Tokyo, Japan) camera and Image Reader LAS-4000 v2.0 software (FujiFilm).

The probe was designed against part of intron 1, which revealed a 6.1 kb WT allele and a 4.5 kb KO allele. The probe was amplified by PCR using the following primers: Big3-F 5'-CCTTGTGCAGATGGATAACC-3' and Big3-R 5'-CTGAGCGAGCAGGAAGTAAT-3') and integrating DIG following manufacturer's instructions (Roche).

RNA isolation.

The retinas and corneas were dissected under a binocular microscope, then rapidly isolated in RNAlater (Ambion; Applied Biosystems, Rotkreuz, Switzerland) before being transferred to TRIzol reagent (Invitrogen AG, Basel, Switzerland) and stored at −80 °C until RNA extraction. Total RNA was extracted according to manufacturer's instructions. Both quantity and quality of RNA were determined on a ND-1000 spectrophotometer (NanoDrop technologies, Inc., Wilmington, DE).

Reverse transcription-PCR and quantitative PCR

cDNA synthesis was performed using 2 µg of total RNA in 20 µl reaction volume. This was performed using an oligo dT primer according to the manufacturer's manual (Affinity Script; Stratagene; Agilent technologies SA, Morges, Switzerland). The equivalent of 50 ng total RNA was used for PCR amplification using the Master Mix (Agilent) with either 250 nM forward and reverse primer pairs, designed to span an intron of the target gene. PCR was performed

with the following cycling conditions: 30 cycles of denaturation at 95°C for 30 sec, annealing at 55°C for 30 sec, and extension at 72°C for 30 sec. Primers sequence was listed in Table 1.

For quantitative PCR, cDNA obtained from 50 ng original total RNA was used for PCR amplification using the 2× brilliant SYBR Green QPCR Master Mix (Agilent) with either 250 nM forward and reverse primer pairs, designed to span an intron of the target gene. Real-time PCR was performed in triplicate in a Mx3000PTM system (Agilent) with the following cycling conditions: 40 cycles of denaturation at 95°C for 30 sec, annealing at 59°C for 30 sec, and extension at 72°C for 30 sec. Quantitative values were obtained by the cycle number (Ct value) reflecting the point at which fluorescence starts to increase above background at a fixed threshold level. Values obtained for the target genes were normalized with the housekeeping gene Gapdh.

Whole cell lysates.

For the preparation of protein extracts -from retina, cornea as well as from cultured cells-, cell pellets were dislodged into cold lysis buffer (20mM Tris-acetate pH 7.0, 0.27M sucrose, 1mM EDTA, 1mM EGTA, 50mM sodium fluoride, 1%Triton X-100, 10mM β-glycero-phosphate, 1mM DTT, 10mM p-nitrophenyl-phosphate, and antiproteases), and centrifuged at 15,000 rpm for 20 minutes. Supernatants were recovered and stored at –70°C until use. Total protein in cell lysates was quantified using the BCA Protein Assay according to the manufacturer (Life Technologies, Carlsbad, CA, USA).

Western blotting experiments.

Equal quantities of total protein lysates (40 ug per well) were resolved by 8-15% SDS-polyacrylamide gel electrophoresis and electrotransferred onto polyvinylidene difluoride membranes. Nonspecific protein binding was blocked by incubating the membrane with a blocking solution (1x TBS, 0.1% Tween 20, 5% nonfat dried milk powder) for 1 h at room

temperature. The blots were then probed with primary antibodies overnight. The immune complex was detected using a peroxidase-conjugated secondary antibody and the chemioluminescent detection kit according to manufacturer's specifications (EMD Millipore EMD Millipore, Merck KGaA, Darmstadt, Germany). FUJIFILM Multi Gauge software was used for densitometric analysis.

Microscopy

Fluorescence microscopy was performed on a Leica DM6000B Microscope, equipped with a Leica DFC365 FX digital camera. Images were captured using the Leica Application Suite (LAS-AF) microscope software. Representative pictures were taken from central areas of the retina using a 40x/0,85 Leica HC PL-APOCHROMAT objective.

For quantifications of INL/ONL thickness, nuclei counting and TUNEL assays, pictures were captured in the posterior pole of the retina, once ventrally and once dorsally to the optic nerve head. Three sagittal sections from three different animals for each genotype and age were analyzed.

Immunohistochemistry.

At necroscopy, the entire eye was removed and fixed in 4 % paraformaldehyde/PBS for 1h followed by cryoprotection in 30 % sucrose/PBS overnight. Eyes were then embedded in 30% albumin egg, 3 % gelatin (Yazzula buffer) and then frozen.

Ten µm-embedded frozen sections were further processed for immunohistochemistry. Briefly, frozen retina sections were blocked in PBS with 2% normal goat serum (Sigma, Buchs, Switzerland) and 0.2% Triton X-100 (Sigma) for 1 h at room temperature (RT) and incubated with primary antibodies in the blocking buffer overnight at 4°C. Sections were blocked again in blocking buffer for 30 min at RT prior to incubation with Alexa-Fluor 488 goat anti-mouse or Alexa-Fluor 594 goat anti-rabbit antibodies for 1 h at RT. In colocalization

experiments, we exposed the retina to RPE65 and EZR antibodies for only 1 h. Incubation with secondary antibody alone was used as a negative control. Retinas were further counterstained with DAPI (Invitrogen), followed by three washes in PBS, before being mounted in Citifluor AF1 (Citifluor, London, UK).

Retinal morphology analysis and INL nuclei counting.

Retinal sections were stained with DAPI and images were captured and INL/ONL thickness was measured using the Leica Application Suite (LAS-AF) microscope software. For nuclei counting, an area of 100 µm wide was defined in the pictures used for INL thickness measurement and DAPI-stained nuclei were counted manually.

Terminal dUTP Nick End-Labeling (TUNEL) of fragmented DNA.

DNA strand breaks in cell nuclei were detected by TUNEL assay, according to manufacturer's instructions (Roche) and previously detailed (Hamann et al., 2009). Briefly, frozen retina sections were permeabilized in 0.1% Triton X-100/0.1% sodium citrate for 2 min on ice and incubated with terminal deoxynucleotidyl transferase (TdT) and fluorescein-12-dUTP or TMR-dUTP for 1 h at 37°C. Retinas were further counterstained with DAPI (Invitrogen), followed by three washes in PBS, before being mounted in Citifluor AF1 (Citifluor).

Statistical analysis

All results were expressed as means ±SEM of the indicated number of experiments. For statistical analysis, Student’s t-test was performed and P values of less than 0.05 were considered to be statistically significant.

Results

Generation of Bigh3 knockout mouse

Floxed *Bigh3* transgenic mice were produced using recombinase techniques. A targeting vector was constructed, which contained two loxP sites flanking exon 1 of the *Bigh3* gene and a neomycin cassette flanked by frt sites. The final recombined floxed allele is presented in Fig 1.A. The generation of *Bigh3* KO mouse is described in material and methods. To assess Cre-mediated deletion and inactivation of the targeted gene, *Bigh3* expression was analyzed at RNA and protein level in the cornea, known to abundantly express this gene. RT-PCR amplification from the first to the third exon showed no amplification in cornea (Fig 2.A). However, when primers spanning exons 4-17 were used, amplicons were detected (Fig 2.A). These data suggest that we succeeded in deleting the first exon of *Bigh3*, but an alternative transcript was nevertheless produced downstream of exon 3. In silico studies revealed a potential in frame start codon in the fourth exon. We therefore assessed whether a truncated protein was expressed resulting from this alternative mRNA by western blotting and immunohistochemistry. Using antibodies raised against amino acids 426-682 of the protein (KE2), the native 68 kDa BIGH3 protein was detected in the cornea of WT mouse, while no protein, even of smaller size, was found in *Bigh3* KO mouse (Fig 2.B). Immunohistochemistry performed on corneas of 1-month-old mice showed that BIGH3 was abundant in the stroma of WT cornea, while expression was completely abolished in *Bigh3*$^{-/-}$ mouse. (Fig 2.C). Although BIGH3 is highly expressed in the cornea and mutations in human are associated with various forms of corneal dystrophy, deletion of *Bigh3* did not perturb corneal development (data not shown). General anatomical studies of *Bigh3*$^{-/-}$ mouse showed no difference when compared to wild type C57/BL6N mouse. They undergo similar development, and no variation was noticed in size or weight of age-comparable animals (data not shown).

BIGH3 expression in mouse retina

Although BIGH3 expression has been well characterized in the cornea of many different animals and human, its precise expression in the retina has never been explored. We therefore performed immunohistochemistry on WT and *Bigh3*$^{-/-}$ eyes at different ages. We observed that BIGH3 was expressed in the retina at the level of RPE and in the optic nerve sheath (Fig 3.A and 3.D). Co-staining of BIGH3 with two RPE markers, the RPE65 and Ezrin (EZR) proteins which are restricted to the cytoplasmic and the apical part of RPE respectively, allowed us to localize BIGH3 to the RPE basal membrane (Fig 3.B-C). BIGH3 was also detected in cultured ARPE-19 cell line (Fig 3.E), a spontaneously arising retinal pigment epithelial (RPE) cell line derived from the normal eyes of a 19-year-old male, while it was absent from WERI-Rb cells (Fig 3.E)

Effect of Bigh3 deficiency on mouse retina

BIGH3 is a secreted protein involved in ECM. Even though it is produced at the RPE level, the possibility that its secreted form could have an impact on the surrounding cells of the retina has to be considered. We therefore compared the retina morphology of wild type and *Bigh3*$^{-/-}$ mouse at different ages. We observed that *Bigh3* deletion had no impact on the retina organization at P0 and P10. However, we measured a transient increase in the inner nuclear layer (INL) thickness of *Bigh3*$^{-/-}$ retina at P15 compared to P30 (Fig 4.A). As shown in Figure 4.B, the thickness of INL decreased by 40% in WT retina versus 9% in *Bigh3* KO retina between P10 and P15. There was no difference at the level of the outer nuclear layer (ONL). To ensure that the INL thickness difference in *Bigh3*$^{-/-}$ versus WT retina was supported by the difference in cell number, cell nuclei were counted in the INL of WT and *Bigh3* KO mouse at

P15. A 25% increase was observed in the nuclei number in the INL of *Bigh3*$^{-/-}$ retina (Supplementary Fig S2).

A recent study implicated BIGH3 in the recruitment of endothelial progenitor cells (EPCs) necessary for angiogenesis (Maeng et al., 2015). In the retina, angiogenesis takes place between P2 and P18, and ECM plays a central role in this process. We were not, however, able to detect any impairment in the retina angiogenesis process in *Bigh3* KO mouse (data not shown).

Bigh3 deficiency promoted ERK survival pathway in the retina

BIGH3 has been implicated in cancer. In two different tumor cell lines, *Bigh3* deficiency has been associated with an elevated proliferation rate and activation of the AKT pathway (Nam et al., 2005; Tumbarello et al., 2012; Wen et al., 2011). Similarly, increased expression of BIGH3 inhibits neuroblastoma cell proliferation and invasion (Becker et al., 2006). We therefore determined whether the loss of *Bigh3* in the retina and the transient increase of cell number in the INL were associated with an increase in AKT activity. We were unable, however, to detect any modulation of the phosphorylation state of AKT in *Bigh3* KO retina compared to WT (Fig 5.A).

The binding of the FAS1 domains of BIGH3 to avβ3 integrin was previously shown to inhibit ERK signaling (Nam et al., 2005). We determined whether the deletion of *Bigh3* in the retina modulates ERK activity. In WT retina, the phosphorylation state of ERK was low at P15 as well as at P30, while it was increased in *Bigh3* KO retina (Fig 5.A-B). JNK and p38, two other members of the MAP kinases were also evaluated and were not modulated in *Bigh3* KO mouse (data not shown). Immunostaining indicated that ERK activity was increased in the

INL of *Bigh3* KO mouse (Fig 5.C). These data would suggest that *Bigh3* deletion transiently affected the apoptotic event in the INL through modulation of the ERK survival pathway.

Apoptotosis in Bigh3$^{-/-}$ mouse

During retina development, most cell types are produced in excess. Apoptosis is therefore an essential physiological process for determining the final number of neuronal cells in the mature retina (Penfold et al., 1986; Young et al., 1984, Mosinger et al., 1998). As BIGH3 has been shown to be implicated in the apoptosis process via its RGD C-terminal domain, we analyzed the apoptotic event in WT and *Bigh3* KO mouse at P10 and P15. As shown in figure 6.A-B, the number of apoptotic cells was reduced in the INL of *Bigh3* KO retina compared to WT at P10. At P15, apoptosis was almost completely turned off in the INL of both WT and *Bigh3* KO mouse. These results suggest that BIGH3 is involved in the apoptotic process necessary to retina maturation. In the absence of BIGH3, this apoptosis was reduced, leading to transient excessive cell number in the INL at P15.

Bigh3 deficiency had no impact on the expression of the BCL-2 proteins in the retina

The apoptotic process involved in the retina development needs functional pro-apoptotic factors, essentially BAX, BIM and PUMA. Indeed, *Bim* KO mouse exhibit an increase in retinal thickness, and loss of *Bax* or *Puma* leads to an increase in ganglion cells (RGCs), bipolar and amacrine cells in adult retina (Mosinger et al., 1998; Hahn et al., 2003; Doonan et al., 2007; Donovan et al., 2006; Harder et al., 2011). We verified whether BIGH3 had an impact on the expression of these BCL-2 proteins. No effect was measured, either at mRNA (data not shown) or at protein level (Fig 7).

Cell cycle exit and Cyclin D1 (CCND1) regulation in Bigh3$^{-/-}$ mouse

During the first 15 days of life, mouse retina completes its maturation. A single layer, the neuroblastic layer (NBL), consisting of undifferentiated cells is subjected to important reorganization to give rise to a multilayered structure of terminally differentiated cells. During this complex process involving cell fate commitment and differentiation of seven cell types, regulation of cell cycle exit is a crucial event. The difference in INL thickness at P15 led us to investigate potential dysregulation in cell division and cell cycle exit. At this stage, healthy retinal cells should have left the cell cycle and stopped dividing. We therefore looked at the expression of Ki67, a marker for proliferating cells. At birth, Ki67 positive cells were detected in WT and *Bigh3* KO mitotic stratum in the outer margin of NBL (Fig 8.A). This staining was completely lost in the retina of P10 and P15 mice, indicating that mitosis exit was normally occurring in *Bigh3* KO mouse.

It has been observed that *Bigh3* deletion was accompanied with CCND1 upregulation (Wen et al., 2011; Zhang et al., 2009). CCND1 promotes G1 to S phase progression and is known to be the predominant D-cyclin in the developing retina. CCND1 expression is elevated in retinal precursor cells (RPCs) but lost in exited precursors and differentiated cells (Barton et al., 2008; Trimarchi et al., 2008). Inappropriate CCND1 expression may therefore directly alter cell progression through the cell cycle. We were unable, however, to detect any upregulation of *Ccnd1* at both RNA and protein level in *Bigh3$^{-/-}$* compared to WT retina (Fig 8B-C).

To determine whether BIGH3 impacted cell cycle progression by acting on other factors involved in cell cycle control such as cyclin-dependent kinases (CDKs) as well as their regulators, the cyclins (CCN), quantitative RT–PCR analysis was performed. As a control, we quantified the *Cdkn1b* ($p27^{Kip1}$) transcript. In the retina, CDKN1B participates in the

determination of multipotent progenitors to withdraw from the cell cycle, and its expression is preserved in postmitotic Muller glia after P15 to maintain their differentiated state. We were unable to detect any modulation of these factors at RNA level in *Bigh3*$^{-/-}$ compared to WT retina (Fig 8.B).

Discussion

BIGH3, also known as TGFßi, is a secreted protein enhancing ECM and cell interactions and has an impact on various biological processes such as apoptosis, cell growth, cancer, wound healing, migration, and osteogenesis. There have been many previous studies on BIGH3, but its physiologic role in the eye and in other tissues is yet to be entirely understood. To further elucidate its function, we generated a knockout mouse line. *Bigh3* KO animals did not present any apparent macroscopic abnormalities compared to control mice, suggesting that *Bigh3* deletion does not severely impair mouse development. Even in the cornea, where BIGH3 is especially abundant, its silencing did not result in any developmental perturbation or abnormal phenotype.

The evaluation of retina from WT and KO animals allowed us to identify for the first time the presence of BIGH3 in the WT mouse retina, at the RPE level as well as in the optic nerve sheath. BIGH3 localization studies showed expression towards the basal side of the RPE, at the level of the plasma membrane. Here again, *Bigh3* deletion had very few phenotypic impacts. We observed a transient increase in the INL thickness at P15, which was no longer present at P30. The enhanced INL thickness was preceded at P10 by the reduction of the physiological apoptotic process that normally takes place in the INL. Downregulated apoptosis was accompanied by upregulation of the ERK survival pathway. The expression of

the proteins of the BCL-2 family, which play a critical role in the apoptotic process leading to retina maturation, were not impacted by *Bigh3* silencing.

Assuming these results, we suggest that the RPE cells could secrete BIGH3 that under normal physiological conditions would play a role on INL cells by binding onto integrin receptors. Cell signaling triggered by secreted BIGH3 implicates its FAS1 domains and RGD motif, which interact with heterodimeric integrin receptors. BIGH3 has been shown to interact with α3β1, αvβ3, αvβ5, α1β1, α6β4 and α7β1 integrin heterodimers (Kim et al., 2000; Kim et al., 2002; Kim et al., 2003; Nam et al., 2006; Oh et al., 2005; Park et al., 2004; Thapa et al., 2005). While the αvβ3 heterodimer was shown to be absent from mouse retina (Pearce et al., 2007), the expression level of other integrins is not well documented in the retina. Based on Gene expression OMNIBUS (GEO) profile Dataset, Itgαv and Itgβ5 are both present at RNA level in mouse retina and could therefore mediate BIGH3 interaction. However, additional experiments are necessary to verify whether αvβ5 heterodimer colocalizes with BIGH3.

Our *Bigh3* KO animals did not develop any macroscopic phenotype and were not predisposed to carcinogenesis compared to a previous mouse model lacking *Bigh3*, which was shown to develop spontaneous tumors (Zhang et al., 2009). In this model, CCND1 up-regulation was shown to be critical (Wen et al., 2011). It is difficult to say why such up-regulation is absent in the model we developed. The two models are in fact different. In the Zhang model, exons 4 to 6 were deleted and BIGH3 protein was not observed in MEF conditioned medium. However, as with our model, *Bigh3* mRNA was identifiable in MEF, although at a reduced rate. An aberrant intracellular BIGH3 protein could have been present but not observed. Another difference could be in the amount of 129Sv/Ev genetic background left in the Zhang model. This could explain why one model is more prone to develop cancer than the other.

ACKNOWLEDGMENTS

The authors wish to thank Carole Herkenne and Céline Agosti for precious technical assistance and Susan Houghton for her help in editing the manuscript. This research was supported by the Fondation pour la Recherche sur les Maladies Héréditaires.

Declaration of interest: The authors report no conflict of interest. The authors alone are responsible for the content and writing of the paper.

Figures

Figure 1. Transgenic construct and gene targeting

A. Targeting construct used to generate *Bigh3*$^{lox/+}$ mouse. Black arrows, *loxP* sites; grey arrows, *frt* sites, Neo, neomycin selection marker.

B. PCR approach used to screen ES cells that have integrated the construct. First PCR amplified a 5' region going from downstream of the first loxP site to the neomycin resistance gene, and a second PCR amplified a 3' region going from the neomycin resistance gene to 3' upstream of the second loxP site.

C. PCR amplification of the 5' and 3' regions from 6 different ES colonies. +, positive control using plasmid DNA as template; -, water. M indicated the 1kb ladder.

D. PCR and Southern blot approach used to screen the *Bigh3* allele, to distinguish between *Bigh3* WT, *Bigh3*$^{lox/+}$ and *Bigh3*$^{+/-}$ allele. The figure shows the WT allele, the allele with the incorporated construct, and the deleted allele following Cre recombinase action. Primers position and amplicons were indicated, as well as the BamHI (B) restriction sites and the probe used for Southern blotting (grey box).

E. PCR product for *Bigh3* WT (2), *Bigh3*$^{lox/+}$ (1), and *Bigh3*$^{+/-}$ (3) alleles.

F. Southern blot showing WT, *Bigh3*$^{+/-}$ and *Bigh3*$^{-/-}$ mouse.

Figure 2. *Bigh3* expression in cornea

A. RT-PCR analysis of mRNA present in the cornea of WT and *Bigh3*$^{-/-}$ mice. Primers amplifying exons 1-3 and encompassing exon 8-9 were used. Gapdh was used as control.

B. Western blot experiment was conducted on cornea of WT and *Bigh3*$^{-/-}$ mice of 30 and 60 days of age using an anti-BIGH3 antibody (KE2) raised against amino acids 426-682.

C. Verification of *Bigh3* silencing at the protein level in the cornea by IH in WT and *Bigh3*$^{-/-}$ mouse of 30 days of age using anti-BIGH3 antibody.

Experiments were conducted with samples obtained from four different mice.

Figure 3. BIGH3 expression in mice retina and optic nerve

A. BIGH3 was detected by immunofluorescence analysis in the retina of mice at different ages (post-natal day 0 to day 30, P0-P30) at the level of RPE, while it was absent from *Bigh3*$^{-/-}$ mice. IH were performed on retina obtained from three different mice at each time point. A negative control was performed in which the first antibody (anti-BIGH3) was omitted.

B. Immunostaining of BIGH3 (red) and RPE65 proteins (green, a cytoplasmic marker of RPE) in a WT retinal section at the age of postnatal day 30 (P30).

C. Immunostaining of BIGH3 (red) and EZR proteins (green, a marker for the apical side of RPE) in a WT retinal section at the age of postnatal day 30 (P30).

D. BIGH3 was detected by IH in the optic nerve sheath of mice at day 10 and 15 (P10, P15), while it was absent from *Bigh3*$^{-/-}$ mice. IH were performed on retina obtained from three different mice at each time point.

E. BIGH3 was detected in ARPE-19 cell line by western blotting using anti-BIGH3 antibody, while it was absent from healthy retina isolated without RPE (HR) and from the WERI-Rb human photoreceptor cell line. The stable HeLa cell line expressing GFP-BIGH3 was used as a positive control.

Figure 4. *Bigh3* KO transiently impacted INL thickness

A. Histologic analysis of the retinas of WT and *Bigh3* KO mouse at day 15 following birth (P15) revealed an increase in INL thickness, while no difference was observed at the ONL level.

B. INL and ONL thickness was measured in WT and *Bigh3* KO retina at day 10 and 15 after birth (P10, P15). Data are the mean ±SEM of three measurements performed on three different retinas. **, $P < 0.001$ WT vs *Bigh3* KO at P10.

Figure 5. AKT and ERK activity in the retina of WT and *Bigh3* KO mouse.

AKT and ERK activity was determined by western Blotting (A) using anti-P-AKT and anti-P-ERK antibodies and normalized against AKT, ERK and Actin (A and B). Data are the mean ±SEM of experiments performed on proteins extracts from five different retinas for each condition, *P<0.02 WT vs *Bigh3* KO at P15 and P30.

C. Immunostaining of P-ERK in the retina of WT and *Bigh3* KO mice at the age of postnatal day 30 (P30).

Figure 6. Apoptosis was reduced in the INL of *Bigh3* KO mice

TUNEL assay (A) and counting (B) of TUNEL-positive apoptotic cells in the INL showed that apoptotic events were increased in *Bigh3* KO retina. Results are expressed as mean ± SEM of 3 different retinas for each group, *p<0.014 WT vs *Bigh3* KO at P10. ONL, outer nuclear layer; INL, inner nuclear layer; GCL, ganglion cell layer.

Figure 7. Expression of BCL-2 proteins in the retina of WT and *Bigh3* KO mouse.

Protein level of BAX, BIM and PUMA was investigated by western blotting in P0 and P15 WT and *Bigh3* KO mouse retina. Protein amounts were normalized with Actin and results are expressed as mean ± SEM of 4 different retinas for each condition

Figure 8. Expression of Ki67 and Ccnd1 during retinal development.

A. Cryosections of WT and *Bigh3* KO retina were labeled with anti-Ki67 antibody. The white arrows indicate the cells positive for the staining.

B. Transcriptional expression of Ccnd1, Cdk1, Cdk2, Cdk4, Cdk6, Ccna2, Ccnb1, Ccnb2 and Cdkn1b was investigated by qPCR in P0, P15 and P30 WT and *Bigh3* KO mice retina. Results are expressed as mean ± SEM of 3 experiments performed in triplicate.

C. Cryosections of WT and *Bigh3* KO retina were labeled with anti-CCND1 antibody. Experiments were conducted on three retinas.

References

Bae, J.S., Lee, S.H., Kim, J.E., Choi, J.Y., Park, R.W., Yong, Park J., Park, H.S., Sohn, Y.S., Lee, D.S., Bae, Lee, E., Kim, I.S., 2002. Betaig-h3 supports keratinocyte adhesion, migration, and proliferation through alpha3beta1 integrin. Biochem. Biophys. Res. Commun. 294, 940-948.

Barton, K.M., Levine, E.M., 2008. Expression patterns and cell cycle profiles of PCNA, MCM6, Cyclin D1, Cyclin A2, Cyclin B1 and phosphorylated histone H3 in the developing mouse retina. Dev. Dynamics. 237, 672-682.

Becker, J., Erdlenbruch, B., Noskova, I., Schramm, A., Aumailley, M., Schorderet, D.F., Schweiger, L., 2006. Keratoepithelin suppresses the progression of experimental human neuroblastomas. Cancer Res. 66, 5314-5321.

Billings, P.C., Whitbeck, J.C., Adams, C.S., Abrams, W.R., Cohen, A.J., Engelsberg, B.N., Howard, P.S., Rosenbloom, J., 2002. The transforming growth factor-beta-inducible matrix protein (beta)ig-h3 interacts with fibronectin. J. Biol. Chem. 277, 28003–28009.

Buchholz, F., Refaeli, Y., Trumpp, A., Bishop, J.M., 2000. Inducible chromosomal translocation of AML1 and ETO genes through Cre/loxP-mediated recombination in the mouse. EMBO. Rep. 1, 133–139.

Chang, B., Hurd, R., Wang, J., Nishina, P., 2013. Survey of common eye diseases in laboratory mouse strains. Invest Ophthalmol Vis Sci. 24;54(7):4974-81.

Donovan, M., Doonan, F., Cotter, T.G., 2006. Decreased expression of pro-apoptotic Bcl-2 family members during retinal development and differential sensitivity to cell death. Dev. Biol. 291, 154-169.

Doonan, F., Donovan, M., Gomez-Vicente, V., Bouillet, P., Cotter, T.G., 2007. Bim expression indicates the pathway to retinal cell death in development and degeneration. J. Neurosci. 27, 10887-10894.

El Kochairi, I., Letovanec, I., Uffer, S., Munier, F.L., Chaubert, P., Schorderet, D.F., 2006. Systemic investigation of keratoepithelin deposits in TGFBI/BIGH3-related corneal dystrophy. Mol. Vis. 12, 461-6.

Ferguson, J.W., Mikesh, M.F., Wheeler, E.F., LeBaron, R.G., 2003. Developmental expression patterns of beta-ig (betaig-h3) and its function as a cell adhesion protein. Mech. Dev. 120, 851–864.

Hahn, P., Lindsten, T., Ying, G.S., Bennett, J., Milam, A.H., Thompson, C.B., Dunaief, J.L. 2003. Proapoptotic bcl-2 family members, Bax and Bak, are essential for developmental photoreceptor apoptosis. Invest. Ophthalmol. Vis. Sci. 44, 3598–3605.

Hanssen, E., Reinboth, B., Gibson, M.A., 2003. Covalent and non-covalent interactions of betaig-h3 with collagen VI. Beta ig-h3 is covalently attached to the amino-terminal region of collagen VI in tissue microfibrils. J. Biol. Chem. 278, 24334–24341.

Harder, J.M., Libby, R.T., 2011. BBC3 (PUMA) regulates developmental apoptosis but not axonal injury induced death in the retina. Mol Neurodegener. 6:50

Hashimoto, K., Noshiro, M., Ohno, S., 1997. Characterization of a cartilage-derived 66-kDa protein (RGD-CAP/Big-h3) that binds to collagen. Biochim. Biophys. Acta. 1355, 303–314.

Hourihan, R.N., O'Sullivan, G.C., Morgan, J.G., 2003. Transcriptional gene expression profiles of oesophageal adenocarcinoma and normal oesophageal tissues. Anticancer Res. 23, 161–165.

Hu, Y.C., Lam, K.Y., Law, S., Wong, J., Srivastava, G., 2001. Profiling of differentially expressed cancer-related genes in esophageal squamous cell carcinoma (ESCC) using human cancer cDNA arrays: overexpression of oncogene MET correlates with tumor differentiation in ESCC. Clin. Cancer. Res. 7, 3519–3525.

Hummler, E., Barker, P., Gatzy, J., Beermann, F., Verdumo, C., Schmidt, A., Boucher, R., Rossier, B.C., 1996. Early death due to defective neonatal lung liquid clearance in α-ENaC-deficient mice. Nat. Genet. 12, 325–328.

Kim, J.E., Kim, S.J., Lee, B.H., Park, R.W., Kim, K.S., Kim, I.S., 2000. Identification of motifs for cell adhesion within the repeated domains of transforming growth factor-beta-induced gene, betaig-h3. J. Biol. Chem. 275, 30907–30915.

Kim, J.E., Jeong, H.W., Nam, J.O., Lee, B.H., Choi, J.Y., Park, R.W., Park, J.Y., Kim, I.S., 2002. Identification of motifs in the fasciclin domains of the transforming growth factor-beta-induced matrix protein betaig h3 that interact with the alphavbeta5 integrin. J. Biol. Chem. 277, 46159–46165.

Kim, J.E., Kim, S.J., Jeong, H.W., Lee, B.H., Choi, J.Y., Park, R.W., Park, J.Y., Kim, I.S., 2003. RGD peptides released from beta ig-h3, a TGF-beta-induced cell-adhesive molecule, mediate apoptosis. Oncogene. 22, 2045-2053.

Korvatska, E., Henry, H., Mashima, Y., Yamada, M., Bachmann, C., Munier, F.L., Schorderet, D.F., 2000. Amyloid and non-amyloid forms of 5q31-linked corneal dystrophy resulting from kerato-epithelin mutations at Arg-124 are associated with abnormal turnover of the protein. J. Biol Chem. 275(15), 11465-11469.

LeBaron, R.G., Bezverkov, K.I., Zimber, M.P., Pavele, R., Skonier, J., Purchio, A.F., 1995. Beta IG-H3, a novel secretory protein inducible by transforming growth factor-beta, is present in normal skin and promotes the adhesion and spreading of dermal fibroblasts in vitro .J. Invest. Dermatol. 104, 844–849.

Maeng, Y.S., Choi, Y.J., Kim, E.K., 2015 TGFBIp regulates differentiation of EPC (CD133+ C-kit+ Lin- cells) to EC through activation of the Notch signaling pathway. Stem Cells. 2015 Mar 18.

Munier, F.L., Korvatska, E., Djemaï, A., Le Paslier, D., Zografos, L., Pescia, G., Schorderet, D.F., 1997. Kerato-epithelin mutations in four 5q31-linked corneal dystrophies. Nat Genet. 15(3), 247-51.

Morand, S., Buchillier, V., Maurer, F., Bonny, C., Arsenijevic, Y., Munier, F.L., Schorderet, D.F., 2003. Induction of apoptosis in human corneal and HeLa cells by mutated bigh3. Invest. Ophthalmol. Vis. Sci. 44, 2973–2979.

Mosinger, Ogilvie, J., Deckwerth, T.L., Knudson, C.M., Korsmeyer, S.J., 1998. Suppression of developmental retinal cell death but not of photoreceptor degeneration in Bax-deficient mice. Invest. Ophthalmol. Vis. Sci. 39, 1713-1720.

Nam, J.O., Kim, J.E., Jeong, H.W., 2003. Identification of the avh3 integrin-interacting motif of Big-h3 and its antiangiogenic effect. J. Biol. Chem. 278, 25902–25909.

Nam, J.O., Jeong, H.W., Lee, B.H., Park, R.W., Kim, I.S., 2005. Regulation of tumor angiogenesis by fastatin, the fourth FAS1 domain of betaig-h3, via alphavbeta3 integrin. Cancer Res. 65(10), 4153-4161.

Nam, E.J., Sa, K.H., You, D.W., Cho, J.H., Seo, J.S., Han, S.W., Park, J.Y., Kim, S.I., Kyung, H.S., Kim, I.S., Kang, Y.M., 2006. Up-regulated transforming growth factor beta-inducible gene H3 in rheumatoid arthritis mediates adhesion and migration of synoviocytes through alpha v beta3 integrin: Regulation by cytokines. Arthritis Rheum. 54, 2734–2744.

Notterman, D.A., Alon, U., Sierk, A.J., Levine, A.J., 2001. Transcriptional gene expression profiles of colorectal adenoma, adenocarcinoma, and normal tissue examined by oligonucleotide arrays. Cancer Res. 61, 3124–3130.

Oh,J.-E., Kook,J.-K. and Min,B.-M., 2005. Beta ig-h3 induces keratinocyte differentiation via modulation of involucrin and transglutaminase expression through the integrin alpha3beta1 and the phosphatidylinositol 3-kinase/Akt signaling pathway. J. Biol. Chem. 280, 21629–21637.

Park,S.-W., Bae,J.-S., Kim,K.-S., Park,S.-H., Lee,B.-H., Choi,J.-Y., Park,J.-Y., Ha,S.-W., Kim,Y.-L., Kwon,T.-H., 2004. Beta ig-h3 promotes renal proximal tubular epithelial cell adhesion, migration and proliferation through the interaction with alpha3beta1 integrin. Exp. Mol. Med. 36, 211–219.

Pearce, J.W., Janardhan, K.S., Caldwell, S., Singh, B., 2007. Angiostatin and integrin alphavbeta3 in the feline, bovine, canine, equine, porcine and murine retina and cornea. Vet. Ophthalmol. 10(5), 313-319.

Penfold, P.L., Provis, J.M., 1986. Cell death in the development of the human retina: phagocytosis of pyknotic and apoptotic bodies by retinal cells. Graefe Arch. Clin. Exp. Ophthalmol. 224, 549–553.

Reinboth, B., Thomas, J., Hanssen, E., Gibson, M.A., 2006. Beta ig-h3 interacts directly with biglycan and decorin, promotes collagen VI aggregation, and participates in ternary complexing with these macromolecules. J. Biol. Chem. 281, 7816–7824.

Sambrook, J., Fritsch, E.F., and Maniatis, T., 1989. Molecular cloning: a laboratory manual. New York: Cold spring harbor laboratory press.

Sasaki, H., Kobayashi, Y., Nakashima, Y., Moriyama, S., Yukiue, H., Kaji, M., Kiriyama, M., Fukai, I., Yamakawa, Y., Fujii, Y., 2002. BIGH3, a transforming growth factor-hinducible gene, is overexpressed in lung cancer. Jpn. J. Clin. Oncol. 32, 85–89.

Sauer, B., 1998. Inducible gene targeting in mice using the Cre/lox system. Methods. 14, 381-392.

Thapa, N., Kang, K.B., Kim, I.S., 2005. Beta ig-h3 mediates osteoblast adhesion and inhibits differentiation. Bone. 36, 232–242.

Skonier, J., Neubauer, M., Madisen, L., Bennett, K., Plowman, G.D., Purchio, A.F., 1992. cDNA cloning and sequence analysis of hig-h3, a novel gene induced in a human adenocarcinoma cell line after treatment with transforming growth factor-h. DNA Cell Biol. 11, 511–522.

Trimarchi, J.M., Stadler, M.B., Cepko, C.L., 2008 Individual retinal progenitor cells display extensive heterogeneity of gene expression. PLoS ONE. 3:e1588.

Tumbarello, D.A., Temple, J., Brenton, J.D., 2012. ß3 integrin modulates transforming growth factor beta induced (TGFBI) function and paclitaxel response in ovarian cancer cells. Moll Cancer. 11:36.

Wen, G., Hong, M., Li, B., Liao, W., Cheng, S.K., Hu, B., Calaf, G.M., Lu, P., Partridge, M.A., Tong, J., Hei, T.K., 2011. Transforming growth factor-β-induced protein (TGFBI) suppresses mesothelioma progression through the Akt/mTOR pathway. Int. J. Oncol. 39, 1001-1009.

Young, R.W., 1984. Cell death during differentiation of the retina in the mouse. J. Comp. Neurol. 229, 362–373.

Zajchowski, D.A., Bartholdi, M.F., Gong, Y., Webster, L., Liu, H.L., Munishkin, A., Beauheim, C., Harvey, S., Ethier, S.P., Johnson, P.H., 2001. Identification of gene expression profiles that predict the aggressive behavior of breast cancer cells. Cancer Res. 61, 5168–5178.

Zamilpa, R., Rupaimoole, R., Phelix, C.F., Somaraki-Cormier, M., Haskins, W., Asmis, R., LeBaron, R.G., 2009. C-terminal fragment of transforming growth factor beta-induced protein (TGFBIp) is required for apoptosis in human osteosarcoma cells. Matrix Biol. 28, 347-353.

Zhao, Y.L., Piao, C.Q., Hei, T.K., 2003. Tumor suppressor function of Betaig-h3 gene in radiation carcinogenesis. Adv. Space Res. 31, 1575–82.

Zhang, Y., Wen, G., Shao, G., Wang, C., Lin C., Fang, H., Balajee, A.S., Bhagat, G., Hei, T.K., Zhao, Y., 2009. TGFBI deficiency predisposes mice to spontaneous tumor development. Cancer Res. 69, 37-44.

Figure 1

A.

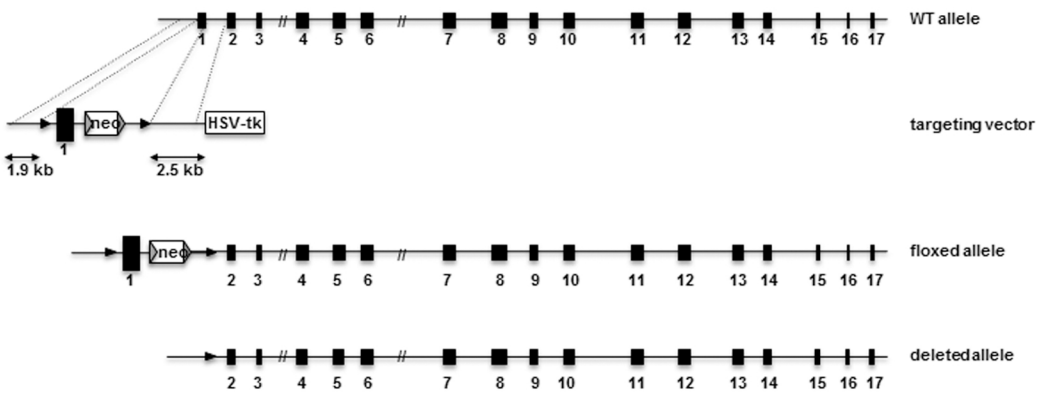
WT allele
1 2 3 4 5 6 7 8 9 10 11 12 13 14 15 16 17
neo
HSV-tk
1
1.9 kb
2.5 kb
targeting vector
floxed allele
deleted allele

B.

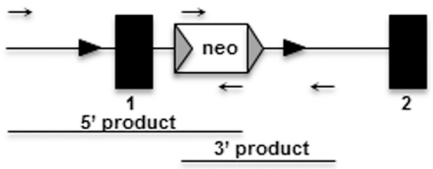
neo
1
2
5' product
3' product

C.

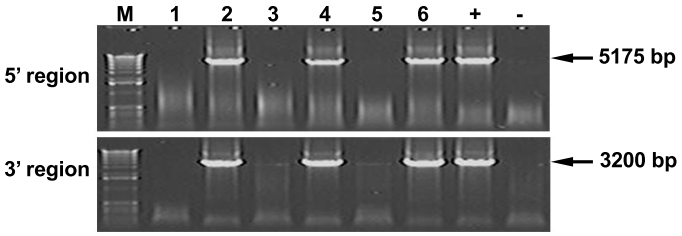
M 1 2 3 4 5 6 + -
5' region
3' region
5175 bp
3200 bp

Figure 1

D.

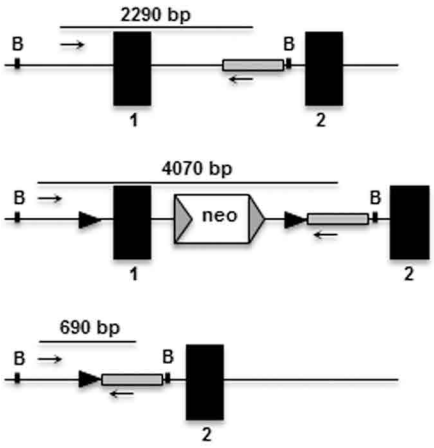
2290 bp
B
B
1
2
4070 bp
B
neo
B
1
2
690 bp
B
B
2

E.

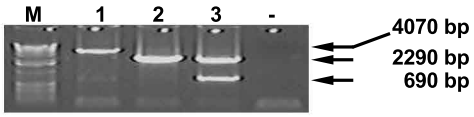
M
1
2
3
-
4070 bp
2290 bp
690 bp

F.

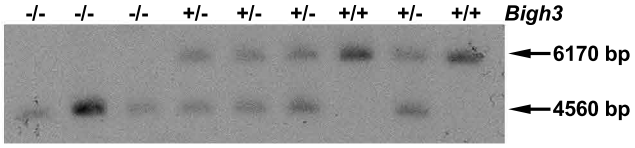
-/-
-/-
-/-
+/-
+/-
+/-
+/+
+/-
+/+
Bigh3
6170 bp
4560 bp

Figure 2

A.

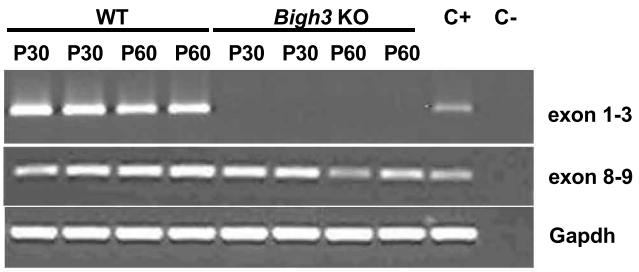
WT
Bigh3 KO
C+
C-
P30 P30 P60 P60 P30 P30 P60 P60
exon 1-3
exon 8-9
Gapdh

B.

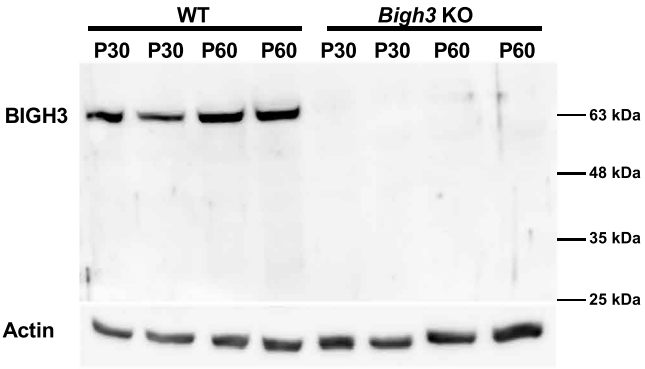
WT
Bigh3 KO
P30 P30 P60 P60 P30 P30 P60 P60
BIGH3
Actin
63 kDa
48 kDa
35 kDa
25 kDa

C.

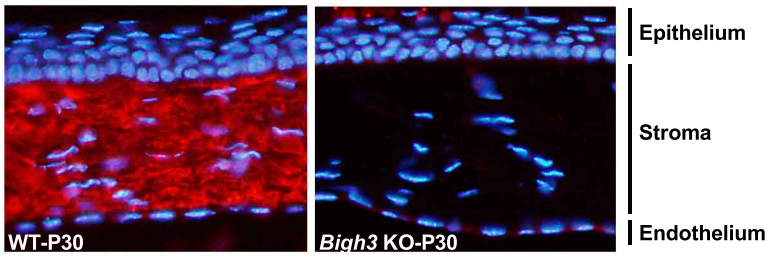
WT-P30
Bigh3 KO-P30
Epithelium
Stroma
Endothelium

Figure 3

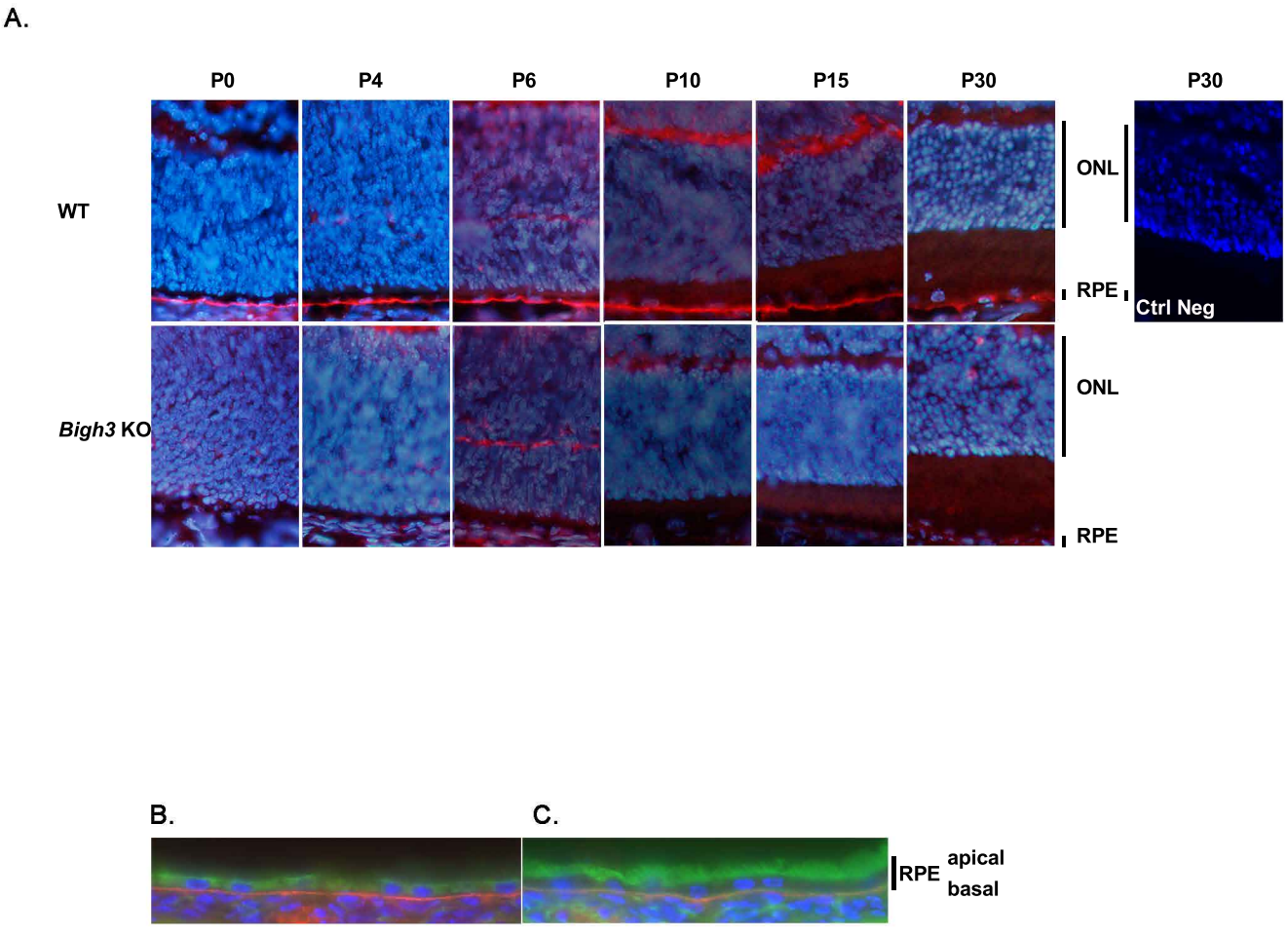
A.
P0
P4
P6
P10
P15
P30
P30
WT
ONL
RPE
Ctrl Neg
Bigh3 KO
ONL
RPE
B.
C.
RPE
apical
basal

Figure 4

A.

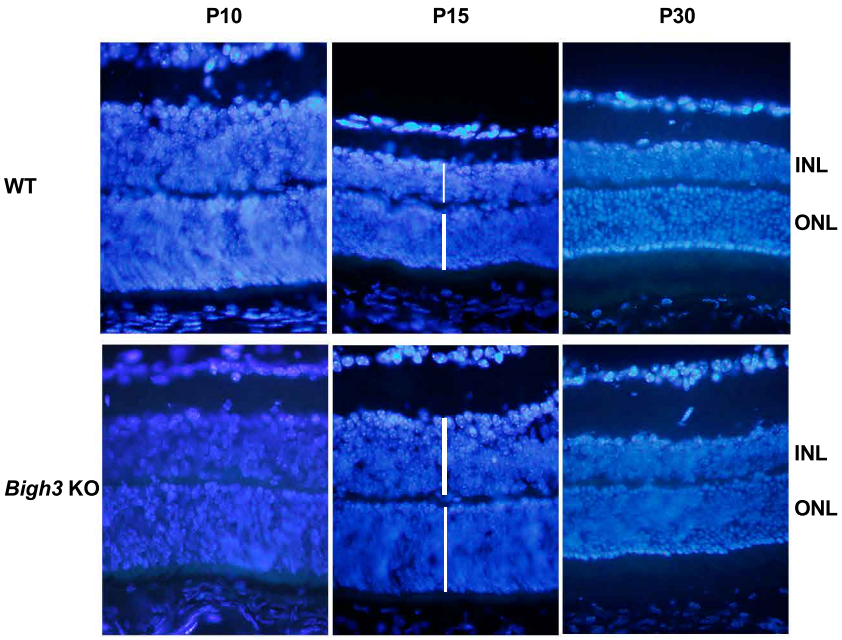
P10
P15
P30
WT
INL
ONL
Bigh3 KO
INL
ONL

B.

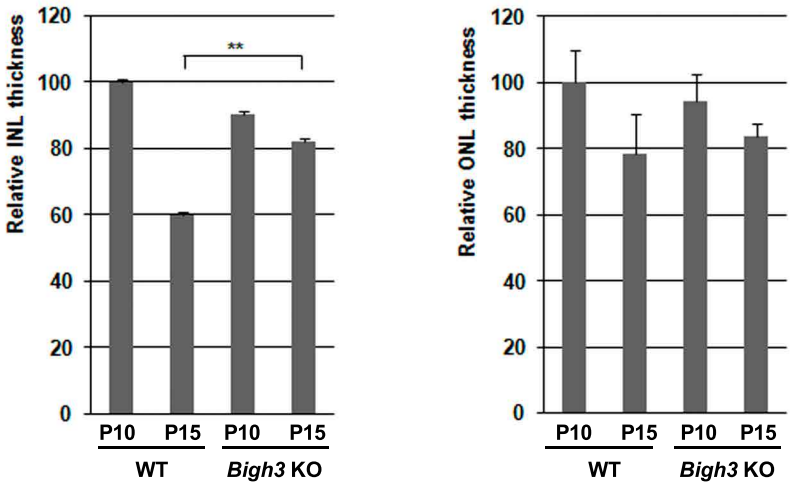
Relative INL thickness
120
100
80
60
40
20
0
**
P10
P15
P10
P15
WT
Bigh3 KO
Relative ONL thickness
120
100
80
60
40
20
0
P10
P15
P10
P15
WT
Bigh3 KO

Figure 5

A.

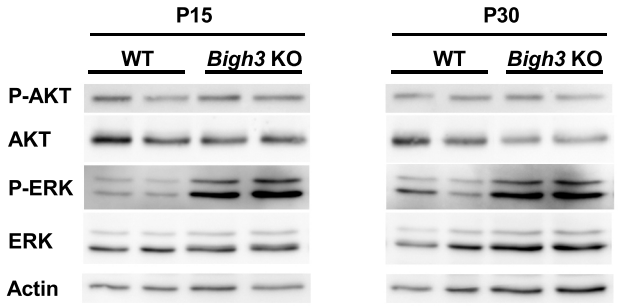
P15
P30
WT
Bigh3 KO
WT
Bigh3 KO
P-AKT
AKT
P-ERK
ERK
Actin

B.

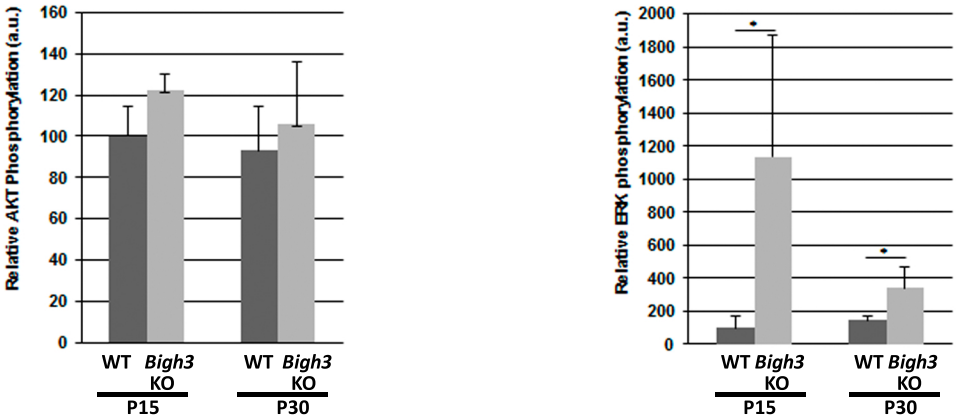
Relative AKT Phosphorylation (a.u.)
160
140
120
100
80
60
40
20
0
WT Bigh3 KO
P15
WT Bigh3 KO
P30
Relative ERK phosphorylation (a.u.)
2000
1800
1600
1400
1200
1000
800
600
400
200
0
WT Bigh3 KO
P15
WT Bigh3 KO
P30

C.

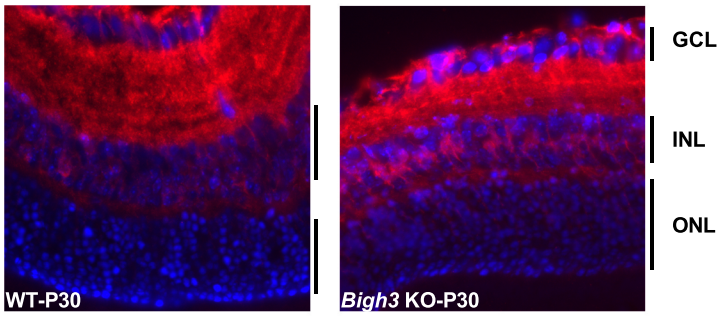
WT-P30
Bigh3 KO-P30
GCL
INL
ONL

Figure 6

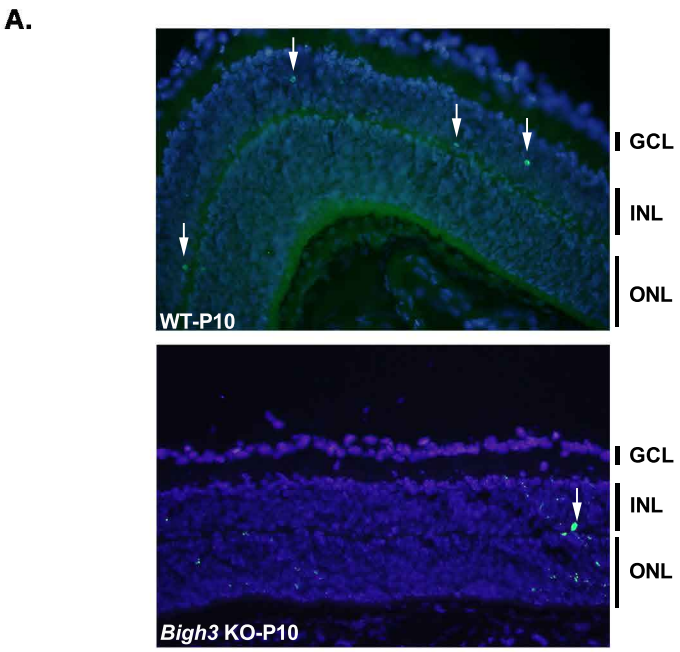
A.
WT-P10
GCL
INL
ONL
Bigh3 KO-P10
GCL
INL
ONL
B.
Relative apoptosis (TUNEL)
30
25
20
15
10
5
0
WT
Bigh3 KO
WT
Bigh3 KO
P10
P15

Figure 7

A.

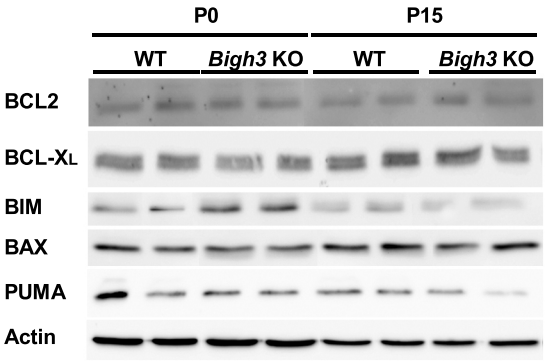
P0
P15
WT
Bigh3 KO
WT
Bigh3 KO
BCL2
BCL-XL
BIM
BAX
PUMA
Actin

B.

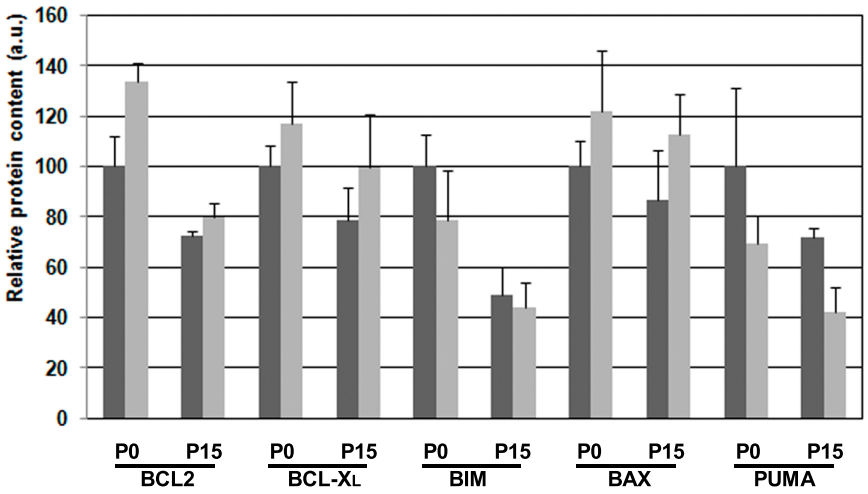
Relative protein content (a.u.)
160
140
120
100
80
60
40
20
0
P0
P15
BCL2
BCL-XL
BIM
BAX
PUMA

Figure 8

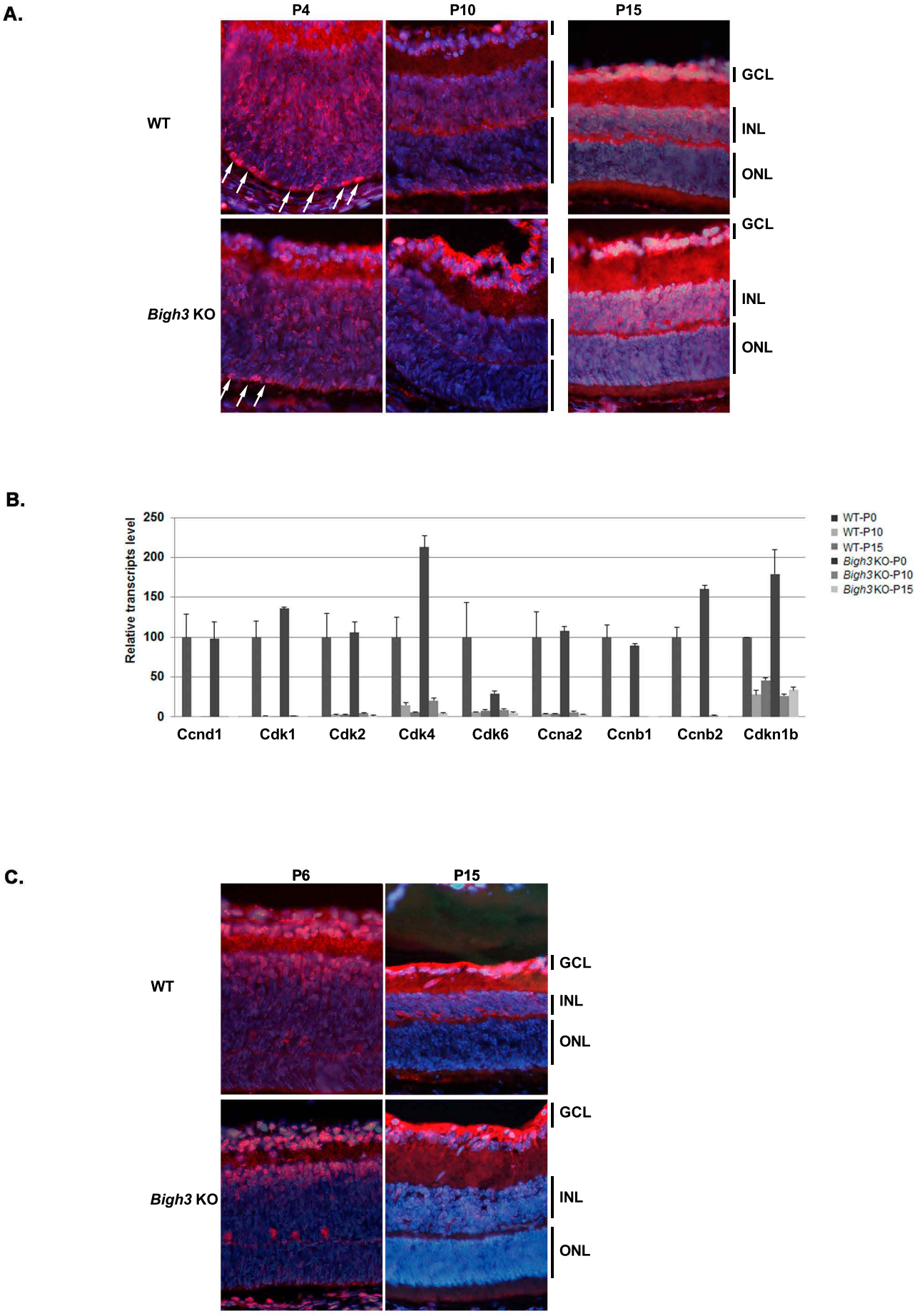
A.
P4
P10
P15
WT
Bigh3 KO
GCL
INL
ONL
B.
Relative transcripts level
250
200
150
100
50
0
Ccnd1
Cdk1
Cdk2
Cdk4
Cdk6
Ccna2
Ccnb1
Ccnb2
Cdkn1b
WT-P0
WT-P10
WT-P15
Bigh3KO-P0
Bigh3KO-P10
Bigh3KO-P15
C.
P6
P15
WT
Bigh3 KO
GCL
INL
ONL